RATE AND ISOTOPIC EFFECTS FOR CONVERSION

OF ICE NANOCRYSTALS TO THE

AMMONIA MONOHYDRATE

By

NEVIN URAS

Bachelor of Science

Anadolu University

Eskisehir, Turkey

1993

Submitted to the Faculty of the
Graduate College of the
Oklahoma State University
in partial fulfillment of
the requirements for
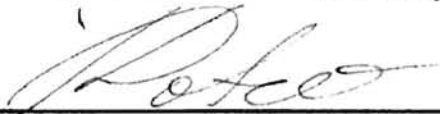the Degree of
MASTER OF SCIENCE
July, 1997

RATE AND ISOTOPIC EFFECTS FOR CONVERSION

OF ICE NANOCRYSTALS TO THE

AMMONIA MONOHYDRATE

Thesis Approved:

J. Paul Devlin
Thesis Advisor

Donald L. Thompson

Rafee

Thomas C. Collins
Dean of the Graduate College

ACKNOWLEDGMENTS

TABLE OF CONTENTS

LIST OF TABLES

LIST OF FIGURES

CHAPTER I

LITERATURE REVIEW

Introduction

This thesis considers the formation of the monohydrate of ammonia in view of the mechanism and rate. The usage of ice nanocrystals, as the sample for Fourier Transform Infrared (FT-IR) Spectroscopy, is also described as related to this hydrate formation.

We can find the potential applications of this study in atmospheric chemistry since the ice is the basic component in the atmosphere of the earth and planets. In addition to an existence of H_2O ice, small molecules such as CH_4, N_2, CO_2 and NH_3 were found in planets, comets and interstellar particles. Interaction of these molecules with the ice causes different effects in the atmosphere.[1]

Since knowledge about the atmosphere of the earth and planets is gained through direct observations, laboratory and theoretical studies that supplement the observations are used to explain the planetary chemical processes and the fundamental constants of these processes, such as rate constants, thermodynamic data, spectroscopic constants and so on.[1] From direct observations, supported by the laboratory and theoretical studies, natural events and the composition of the planets and their atmospheres can be predicted.

Lewis[2] made a model for Jupiter's clouds and studied the thermodynamic properties. He showed that solid phases of H_2O and NH_3 are important components of the atmosphere at high altitudes at which the temperature is below a few hundred Kelvin. The thermodynamic studies of the NH_3-H_2O system showed that the hydrate forms of ammonia may be found under the clouds of NH_3.

The same model was assumed for satellites of the outer planets by Lewis.[3] He showed that solid H_2O, NH_3 and its hydrates condense below 250 K.

To our knowledge, there are no kinetic data about the formation of ammonia monohydrate. For this reason, the rate of conversion of ice nanocrystals to the ammonia monohydrate was studied under laboratory conditions. To further understand the nature of this conversion, H_2O ice was replaced by D_2O ice or NH_3 by ND_3. From this point, we have also tried to observe isotopic effects on the reaction rate for this conversion.

The Structure of Ice Nanocrystals and Their Interactions with Adsorbates

In nature, it is the surface of ice that most commonly interacts with other components of the universe. One of the best tools to study ice surface structure with FT-IR spectroscopy is the ice nanocrystals. Methods developed by our group to produce ice nanoparticles have led to contributions to the identification and interpretation of the surface region of the crystalline ice. The information about not only the structure of the ice nanocrystals but also interactions of some small adsorbates with ice nanocrystals is usually derived from difference spectra. The difference spectra can be obtained from comparison of spectra of annealed and unannealed ice or of the bare and adsorbate-coated ice.[4]

When the ice nanocrystals are annealed, the size of the particles becomes bigger by the Ostwald ripening process. During this process, the small particles vaporize and the vapor is added to the surface of the larger ones. Further, one can choose the particle size depending on the annealing temperature (generally, it changes between 110-150K). Some of the surface molecules are converted to the interior ice during the ripening process.

Consequently, after the annealing process, some of the surface molecule absorption is lost due to this conversion. This can be followed by FT-IR difference spectroscopy as decreasing peak intensities of the surface molecules. Although the total amount of ice does not change, different relative amounts of surface and interior absorption are obtained from the annealed and unannealed ice sample spectra that are taken at the same temperature.[5] In addition to the conversion of the surface molecules to the interior ice, some subsurface is also converted to the interior ice because of the ripening process.[8]

The difference spectra, between the annealed and unannealed spectra, and computational methods show that a single ice nanoparticle, with a spectrum consistent with a largely crystalline ice structure, has three parts; surface, subsurface and interior.[4] The surface of ice nanocrystals consists of 3-coordinated molecules with non-H-bonded atoms or dangling-H (D) (or d-H(D)), molecules with a dangling-O coordination (or d-O) and 4-coordinated surface (or s-4) water molecules.[5] In the interior of crystalline ice, each water molecule is coordinated through four H-bonds. Two of them are through the two hydrogen atoms, the others are through oxygen (Figure 1).

Moreover, the three parts of the ice nanocrystals have different vibrational modes that can be identified and distinguished from each other by using the difference spectra. From the difference spectra combined with computational evidence, vibrational modes of the surface molecules are assigned[4] as follows; a) the out-of-phase stretch of the three coordinated molecules with dangling-H (D) is 3692 (2725) cm^{-1}, the in-phase stretch 3110 (2300) cm^{-1} and the bending modes 1650 (1215) cm^{-1}, b) the out-of-phase stretch of the three coordinated molecules with dangling-O is 3560 (2640) cm^{-1}, the in-phase stretch 3350 (2480) cm^{-1} and the bending modes 1690 (1235) cm^{-1}, c) the out-of-phase of s-4

dangling-O (d-O)   dangling-H (d-H)

Surface 4-Coord.
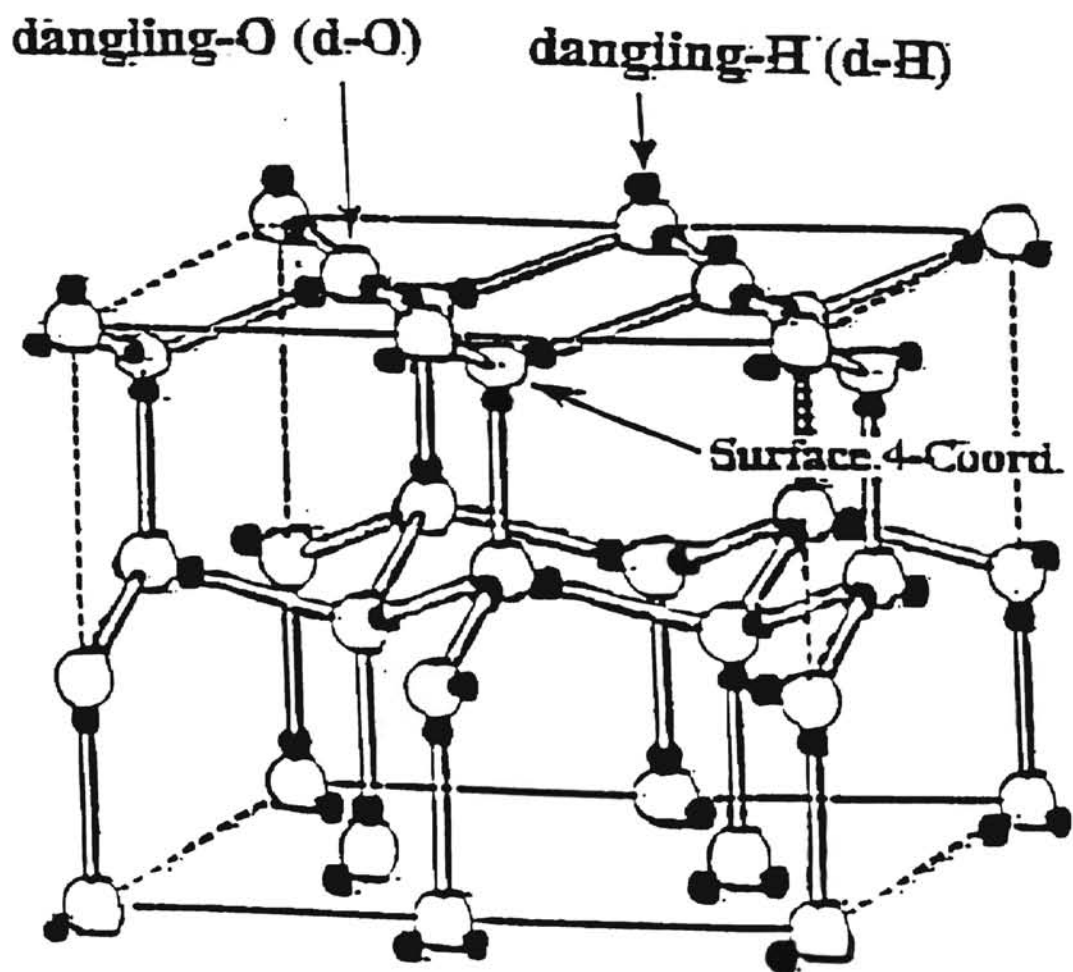
Figure 1. Crystalline ice structure

molecule is 3490 (2580) cm^{-1}, the in-phase 3270 (2430) cm^{-1}. Interior D_2O ice gives

absorption in the 2300-2500 cm^{-1} spectral range. Figure 2 shows the difference spectrum

of D_2O between spectra of small and large nanocrystals. As seen in that figure, positive

bands represent out-of-phase stretch modes for surface molecules including s-4, and the

negative triplet represents the interior ice spectrum.[7]

The interaction of the adsorbates with the ice nanocrystals can also be examined

by obtaining the difference spectra in two ways: one of them is between spectra of small

and large ice particles coated with adsorbates and the other is between spectra of bare ice

and adsorbate-coated ice.[4,5]

As mentioned above, the three parts of the ice nanocrystals are surface,

subsurface, and interior. The adsorbates (used by our group) can be categorized as a)

weak adsorbates, b) strong H-bonding adsorbates and c) penetrating adsorbates,

depending on their effect on the three parts of the ice nanocrystals. Since the subject of

this study is focused on one of the penetrating adsorbates, namely NH_3, they will be

explained in detail. However, the strong H-bonding and the weak adsorbates, particularly,

provide insight to the surface structure of the ice nanocrystals. For this reason, they will

be considered briefly.

The weak adsorbates affect only vibrational modes of the surface molecules of ice

nanocrystals and CH_4, N_2, CO, and H_2 can be given as examples.[5,6,8,9] Since these

adsorbates do not have the capability to form significant H-bonds, they are called weak

adsorbates. They do not affect the subsurface or the interior ice spectra. One more

characteristic of these adsorbates is that they are easily desorbed below 100 K.[5] In Figure

3, the effects of adsorbed N_2, CO and H_2 on the cubic ice spectrum can be seen as shifting
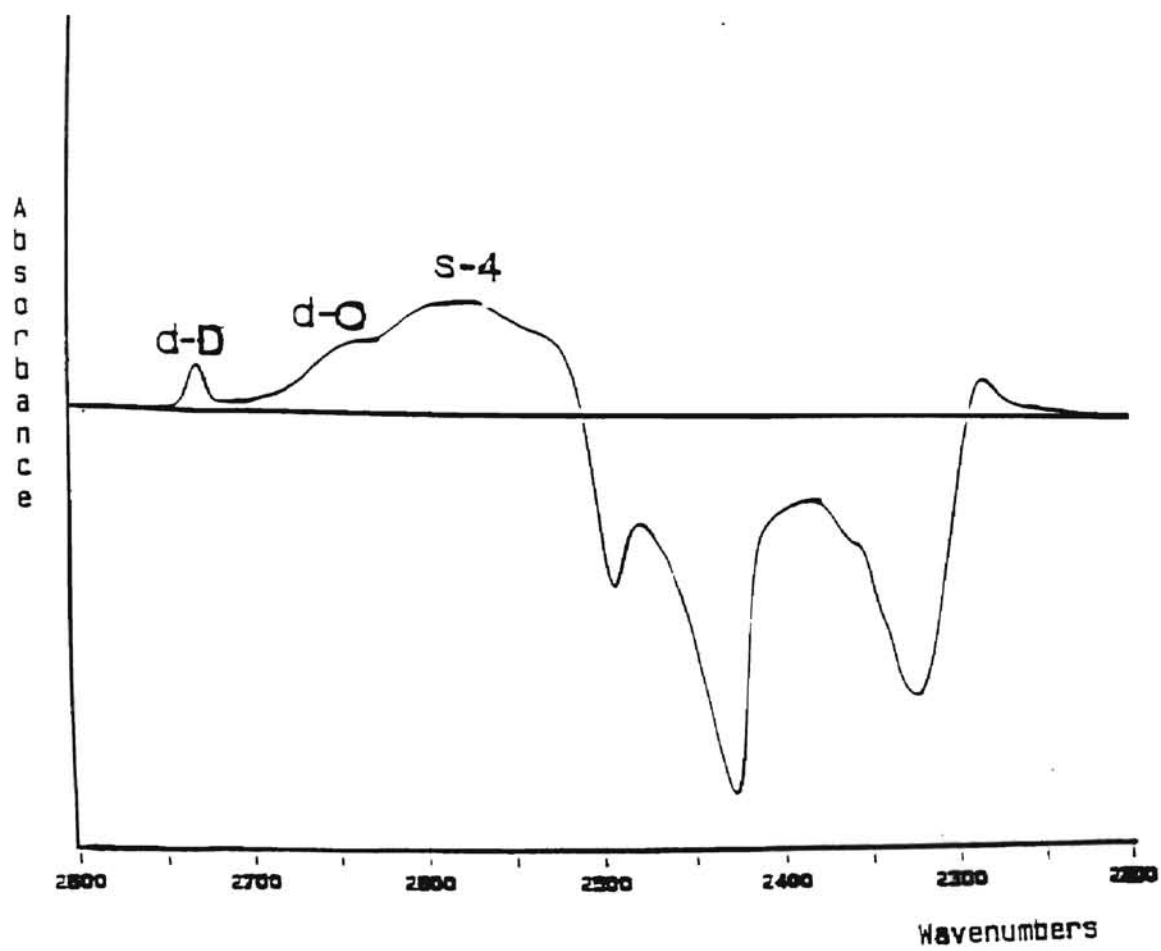
Figure 2. A difference spectrum of D_2O ice from subtraction of annealed nanocrystals from spectrum of unannealed nanocrystals.
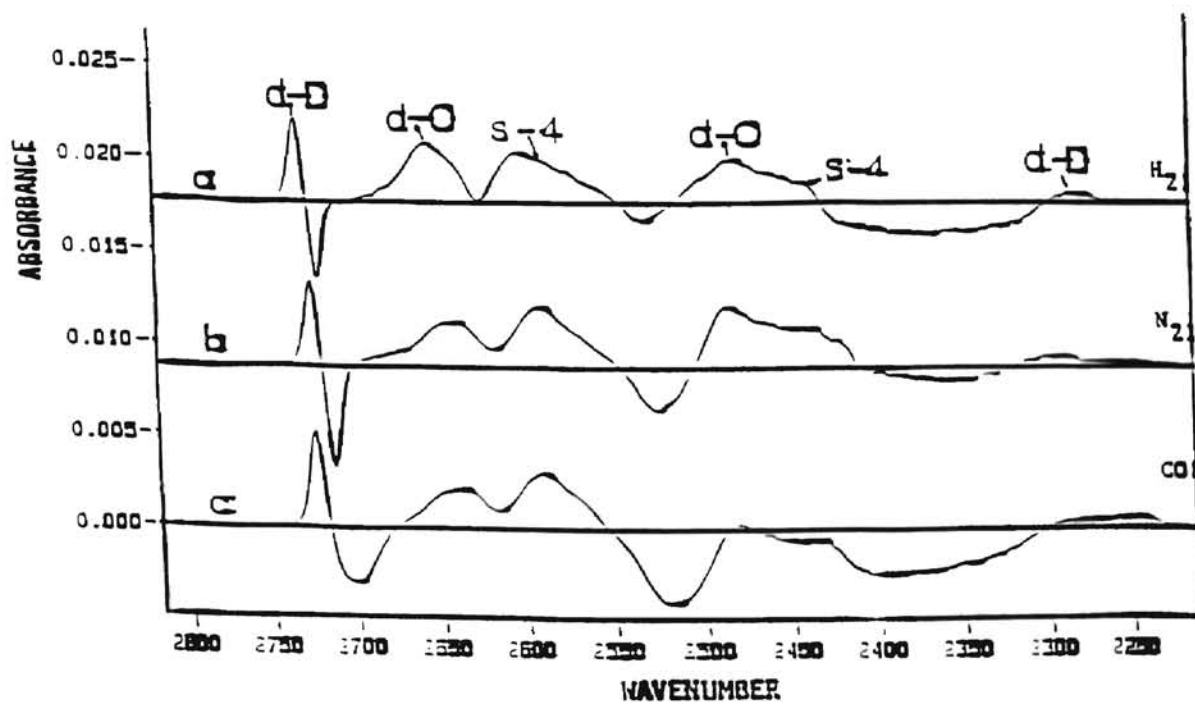
Figure 3. Difference spectra between bare and adsorbate coated D_2O ice nanocrystals for adsorbates H_2, N_2 and CO

the vibrational modes of the surface D_2O molecules.[12]

Among the strong H-bonding adsorbates are H_2S, SO_2, HCN and acetylene. Delzeit[13] studied the interactions of these adsorbates with the surface of ice nanocrystals. He showed that these adsorbates affect the spectrum of the subsurface and interior ice as well as the spectrum of the surface molecules, but without chemically reacting.

The penetrating adsorbates react with ice to form hydrates at cryogenic temperatures.[10] Ethylene oxide, HCl, and NH_3 are in this class of adsorbates. They affect all parts of the ice spectrum and also react with ice nanocrystals to form crystalline hydrates at the cryogenic temperatures.[10] They also do not undergo desorption at cryogenic temperatures.

Delzeit et al.[10] showed that ethylene oxide (EO) penetrates through ice crystals by virtue of its strong proton-acceptor character. Further, they concluded that EO converts the ice nanocrystals to the type I clathrate hydrate via a molecular mechanism. Firstly, the ice nanocrystals were exposed to EO(g) at 125 K at which temperature EO acts as an adsorbate. Then, the temperature was raised to 132 K for the hydrate formation. Total conversion time was found as 3h at 132 K.

In the case of HCl, the conversion of ice nanocrystals to the hydrate of HCl proceeds via an ionic mechanism based upon formation of H_3O^+ and Cl^- ions. The conversion, resulting in formation of the amorphous monohydrate, was completed within 1 hour at 125 K. After warming to 135 K, the reaction product became crystalline nanoparticles of the ionic monohydrate.[10]

In our classification, NH_3 is also a penetrating adsorbate. A study by Delzeit[13] showed that NH_3 reacts with the surface of the ice nanocrystals to form the amorphous

monohydrate of ammonia. He showed that when the ice nanocrystals were exposed to NH_3, NH_3 did not immediately migrate through the interior part. Thus, previous studies of ammonia and ice nanocrystals in our group have been limited to only the surface of the ice nanocrystals not the interior part of it. Since the interest of this study is NH_3 and ice, we will investigate this interaction further.

Studies with NH_3 and H_2O and Their Derivatives

Langet, Caillet and Caffarel[14] showed in their theoretical calculation that, in a dimer structure of NH_3 and H_2O, the dimer containing ammonia as a proton acceptor ($H_3N...HOH$) is much more stable than that containing ammonia as a proton donor ($H_2O...HNH_2$). Further, they showed that since the stability of $H_3N...HOH$ is greater than that of $H_2O...HOH$, NH_3 is a better proton acceptor than H_2O.

Three types of NH_3-H_2O molecular solids have been described in the literature; the monohydrate ($NH_3.H_2O$), hemihydrate ($2NH_3.H_2O$), and dihydrate ($NH_3.2H_2O$).[15,16] As one can see from the molecular formulas, the amount of NH_3 is the determining property. Its capability to form these H-bonded systems is due to its strong proton acceptor character.

Bertie and Shehata[15] studied $NH_3.H_2O$ and $ND_3.D_2O$. They produced spectra of bulk forms of hydrates of ammonia by using the mull technique at 100 K, and interpreted peak values corresponding to vibrational modes for the first time. Figure 4 and Figure 5 (adapted from reference 15) show FT-IR spectra for both $NH_3.H_2O$ and $ND_3.D_2O$, respectively, with corresponding peak values in Table 1. Since in the case of $ND_3.D_2O$,
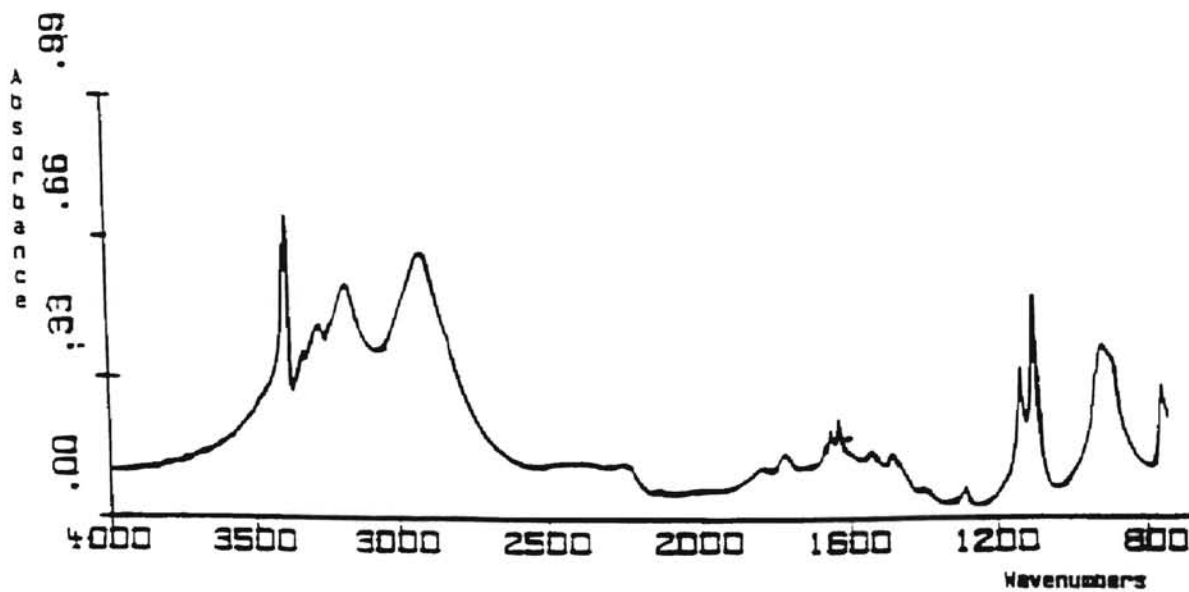
Figure 4. Infrared spectrum of $NH_3.H_2O$ at 100 K (adapted from reference 12)
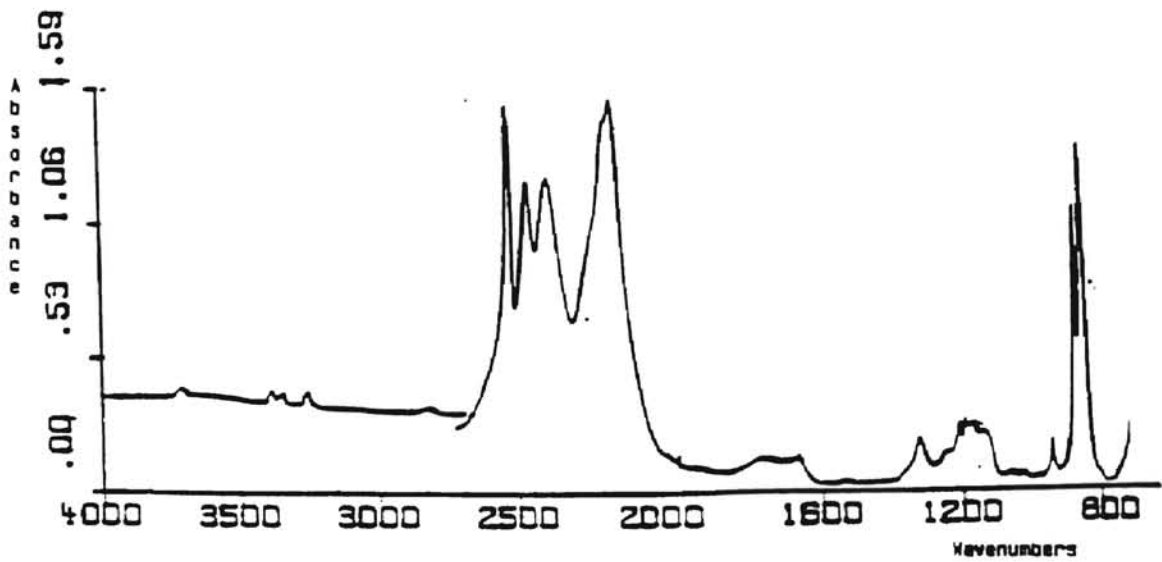
Figure 5. Infrared spectrum of $ND_3 \cdot D_2O$ at 100 K (adapted from reference 12)

Table 1

Vibrational frequencies of $NH_3.H_2O$ and $ND_3.D_2O$

NH₃·H₂O[a]		ND₃·D₂O[a]		
v/cm⁻¹	Intensity	v/cm⁻¹	Intensity	Assignment[b]
~5210	vw			
5015(1)	w	3715(2)	w	$(v_1 + v_3)(a)$
~4953	sh			
~4800	w,br	~3610	sh	
		~3471	vw	
4515(4)	w	3392(2)	w	$(v_1 + v_2)(a)$
2471	w	3362	sh	$v_{NH}(ND_2H)$
2467	w	3349.2(5)	w	or
2464	w	3344.9	sh	$v_{ND}(NH_2D)$
2410	w	3259(2)	w	HDO, $v_{O-H\cdots O}$
		~3135	vw	HDO
~4417	vvw			
~4366	vvw			
~4320	vvw			
~4240	vvw			
~4150	vvw	~3085	vw,br	
~3771	sh	2954	vvw	
3689	sh	2940	vvw	
3590	sh	2917	vvw	
3531	sh			
2197	w	2525(5)	w	HDO, $v_{O-H\cdots N}$
3403.2(5)	vs	2534.3(5)	vs	
3392.1(5)	vs	2526.1(5)	vs	$v_3(a), B_1, B_2$, and B_3
3387.3(5)	vs	2522.2(6)	vs	
3332(2)	s			$v_1(a); 2v_4(a)$
3294	sh			
3275(3)	s	2459(2)	vs	$v_{O-H-O}(B_2$, out-of-phase)
3235	sh	~2414	sh	
3182(2)	vs	2390(1)	vs	$v_{O-H-O}(B_1$, in-phase)
~2950	sh	~2260	sh	
		2189(2)	vs	$v_{O-H\cdots N}(B_1)$
2587(10)	vs	2165(2)	vs	$v_{O-H\cdots N}(B_2)$
		~1929	sh	
		~1836	sh	$3v_R(W); v_R(W) + v_2(W)$
~2430	w,br	1767(3)	mw,br	$v_s(a) + v_R(W)$
2260(3)	w,br	~1675	w,br	
2140.8(5)	vw	1667(1)	mw	$2v_2(a)$
2028(4)	vw,br			
1994(5)	vw,br	1534(2)	vw	$v_1(a) + v_R(W)$
		1467(2)	w	$v_2(HDO)$
1834(3)	w			
1773(3)	w	1319.5(9)	mw	$2v_R(W)$
~1696	sh	1243(3)	mw	$v_2(W); v_R(W) + v_R·(W)$
1665.5(5)	m	~1217	sh	$v_4(a)(B_2)$
1650.1(5)	m	1209.1(5)	mw	$v_4(a)(B_1)$
1627.0(5)	m	1192.6(5)	mw	$v_4(a)(B_3)$
~1594	sh	1169(1)	mw	$v_R(W) + v_R·(W)$
1537(2)	w	1135(3)	mw	$v_R(W) + v_R·(W)$
1480(2)	w			$2v_R·(W)$
1439(4)	w	1060(4)	vw	$2v_R·(W)$
1402(2)	w	1023(2)	vw	$2v_R·(W)$
1287.1(5)	w	943.4(6)	mw	$2v_R·(W)$
1133.4(5)	s	870.6(9)	vs	$v_2(a)(B_1)$
1095.9(5)	vs	848.2(8)	vs	$v_2(a)(B_2)$
		~806	sh	
~932	sh			
915	s	682.3(6)	vs	$v_R(W)$
~893	sh	661(2)	s	

12

their sample contained 1% H, they also observed ND_2H, NH_2D and HOD vibrational modes.

Deuterium Isotope Effects on Reaction Kinetics

When a hydrogen atom in a given molecule is replaced by deuterium, the observable changes are then called "deuterium isotope effects" (DIEs). The deuterium isotope effects have a variety of forms[17, 18], such as the isotope frequency ratio (ν_{AH}/ν_{AD}), the thermodynamic isotope effect (K_H/K_D or $\Delta K_a = pK_a (D_2O) - pK_a (H_2O)$), the kinetic isotope effect (k_H/k_D), vapor pressure isotope effect (P_{AH}/P_{AD}), etc.. Since one interest of this study is to find out the kinetic isotope effect for the conversion of the ice nanocrystals to the monohydrate of ammonia, it will be explained here in detail.

The theoretical explanation of isotope effects on the reaction rates are generally based upon Absolute Reaction Rate Theory (or Transition State Theory).[19] Bigeleisen[20] derived the rate constant ratio for the competitive reaction of the isotopic molecules by using this theory. He started with Eyring's formalism for the rate constants of the reactions ($A_1 + B + \ldots \longrightarrow P_1$ and $A_2 + B + \ldots \longrightarrow P_2$, where A_1 and A_2 are the isotopic molecules, P is the product) that could be written

$$k_1 = K_1 \frac{C_1^{\#}}{C_{A1}C_B\ldots} \left(\frac{kT}{2\pi m_1^*}\right)^{1/2} \frac{1}{\delta_1}$$

$$k_2 = K_2 \frac{C_2^{\#}}{C_{A2}C_B} \left(\frac{kT}{2\pi m_2^*}\right)^{1/2} \frac{1}{\delta_2}$$

13

where K is the transmission coefficient, $C^{\#}$ is the concentration of the activated complex, m^* is the effective masses of the complex along the coordinate of decomposition, and δ is the length of the top of the potential barrier. From these equations, he found k_1/k_2 as $(K_1 C_1^{\#} C_{A2} (m_2^*)^{1/2} / K_2 C_2^{\#} C_{A1} (m_1^*)^{1/2})$ (since δ is the same for isotopic molecules). He replaced the ratios of concentration terms with corresponding ratios of the complete partition functions (Q) constructed from translational. vibrational and rotational partition functions. He chose the minimum of the energy scale as zero in the potential energy curve for both isotopic molecules since the potential energy is invariant for the two isotopic molecules. In the study of Bigeleisen and Mayer[21], they derived the equilibrium constants in terms of the ratio of the complete partition functions. They showed that the only contribution in the ratio of the complete partition functions comes from the vibrational parts since the other terms in the ratio of the partition functions of the two isotopic molecules cancel each other. Bigeleisen[20] obtained the following equation for the rate constants of the two isotopic molecules;

$$\frac{k_1}{k_2} \frac{s_2}{s_1} \frac{s_1^*}{s_2^*} = \frac{K_1}{K_2} \left(\frac{m_2^*}{m_1^*} \right)^{1/2} \left[1 + \sum_i^{3n-6} G(u_i) \Delta u_i - \sum_i^{3n^{'}-6} G(u_i^*) \Delta u_i^* \right]$$

where s is symmetry number, asterisk (*) denotes the transition state, $u_i = h\nu_i/kT$ and $\Delta u_i = h/kT (\nu_{i1} - \nu_{i2})$, h is Planck's constant. k is the Boltzmann constant, T is the temperature, ν is the frequency. As explained in reference 21, G(u) was found to be expressed as $G(u) = 1/2 - 1/u + 1/(e^u - 1)$.

The same procedure was followed by Melander[19] to find the ratio of the rate

constants of the two isotopic molecules and he obtained a similar result. Further, he

derived the formula for the ratio of the rate constants of the isotopic hydrogen in heavy

molecules by making some assumptions. It was shown that the primary hydrogen effect

(of a reaction in which hydrogen is directly involved) can be treated as a zero-point

energy effect and given by this equation;

$$\frac{k_1 \; s_2 \; s_1{}^*}{k_2 \; s_1 \; s_2{}^*} = \exp\left\{\frac{h \, c}{2kT}(\overline{v}_{k(1)} - \overline{v}_{k(2)})\right\},$$

where $\overline{v}$ is the frequency in wave numbers and c is the velocity of the light. Here,

v generally represents the stretching frequencies of a bond, that connects hydrogen and a

second atom, that is broken in the reaction. Although this equation is useful for the

hydrogen isotopes, it cannot be applied to other isotopic species for which the Bigeleisen

formalism can be appropriate.

Figure 6 (modified from reference 22) shows the potential energy diagram and the

zero-point energies for a given reaction of a molecule with H or D.[22] The Hooke's law

expression is given by the following equation:

$$v = (1/2\pi c)\,(\sqrt{k/\mu})$$

where v is the frequency, μ is the reduced mass that is approximately equal to 1 and 2 for

heavy molecules with H and with D, respectively.[22] According to the harmonic oscillator

approximation, energy levels of the harmonic oscillator are given by $E_n = (1/2 + n)\,hv$,

where n is the vibrational quantum number (0, 1, 2, …), h is Planck's constant and v is

the vibrational frequency. Putting n = 0 (because at room temperature or below, most of
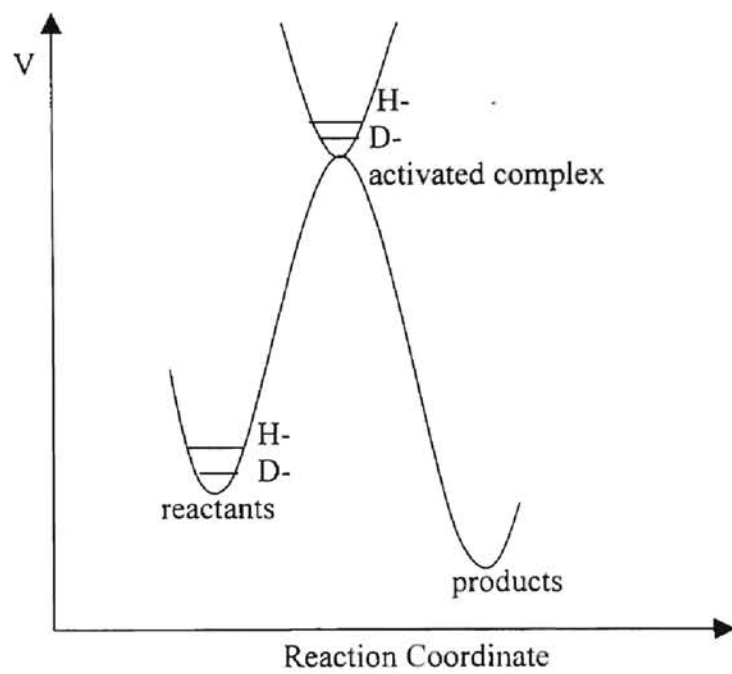
Figure 6. Potential energy (V) diagram for a molecule with H and D

the molecules reside in the ground vibrational state) gives the energy equation as $E = h\nu/2$. Combination of the energy and frequency equations explains why the zero-point energy is different for the isotopic hydrogen. Since the molecule with deuterium has the lower zero-point energy, it is more stable than that with hydrogen due to the dissociation energy differences.[22]

Moreover, when the reactant with hydrogen or deuterium reaches the activated complex point, the bonds between the atom and hydrogen or deuterium become weaker. Consequently, the force constants between the atom and hydrogen or deuterium become smaller (and the vibrational energy is directly proportional to the square root of the force constant). Thus, in the activated complex, the difference between the zero-point energy levels for the molecule with hydrogen and the molecule with deuterium becomes smaller. If one considers the rate process, this difference makes the activation energy for the molecule with deuterium higher than that for molecule with hydrogen. Simply put, the molecule with hydrogen reacts faster than that with deuterium.[22]

The relation between the activation energies and the zero-point energies for the isotopic molecules was found by Bigelesein.[20] He concluded that the difference in activation energies at low temperature resulted from the difference in the zero-point energies between the isotopic molecules and their activated complexes.

The applications of the deuterium isotope effects for different conditions can be found in the references 22 and 23. A discussion of the magnitude of the deuterium isotope effect on the reaction rates was given by Westheimer.[24]

CHAPTER II

EXPERIMENTAL

Introduction

This experimental chapter is divided into two sections: experimental equipment and experimental procedure. The equipment part will be given first so that the procedures can be easily followed.

Experimental Equipment

Experimental equipment mainly consists of a vacuum system, cryogenic system, a cryogenic cell and the FT-IR instrument. The components of the equipment are shown in Figure 7 as a cartoon.

Vacuum System

A Welch Duo Seal vacuum pump model 1402 and an oil diffusion pump were used to evacuate the glass manifold. The manifold was connected to the outer portion and the inner portion of the infrared cell by a vacuum line. The connection between the outer portion and the vacuum system provided a vacuum required in order to isolate the inner portion of the cell from thermal transport. The inner port connection was used for evacuation of the cell and admission of the gaseous samples into the cell. The pressure was measured with a Hastings Vacuum Gauge. The minimum pressure for this system is $\sim 10^{-5}$ torr. Loading of the gaseous samples was monitored using a dual channel Validyne
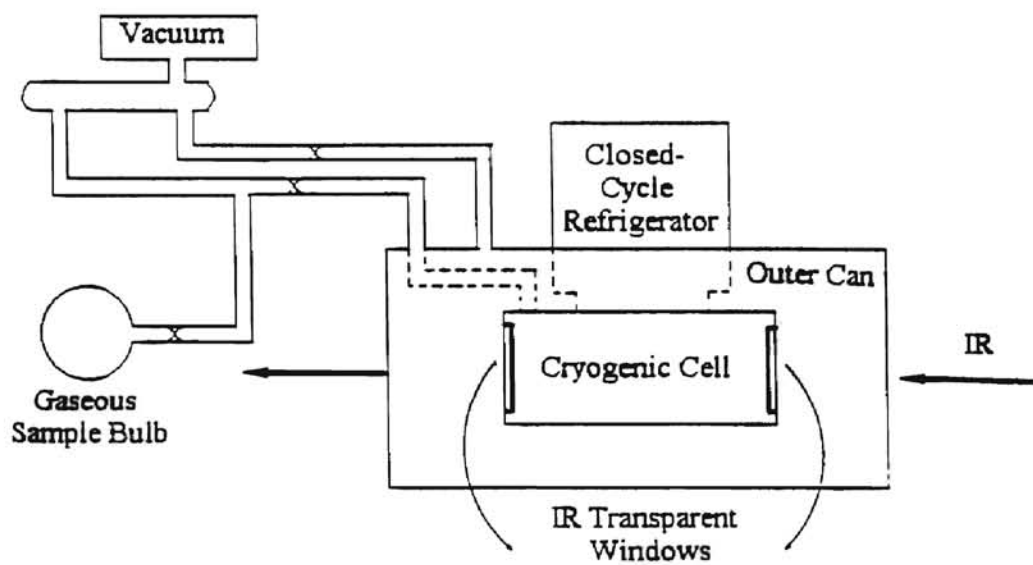
Figure 7. Main components of the experimental equipment

Model CD 223 gauge with the measurable pressure ranges of 0.01 to 150 and 0.1 to 1000 torr, respectively.

Cryogenic System and Cryogenic Cell

The main component of the cryogenic system was an Air Product Model HC-2 water-cooled closed cycle helium refrigerator. The minimum temperature capability was ~10 K depending on the thermal load. The other components of the cryogenic system were a Lake Shore temperature measuring assembly and a hand-coiled 40 ohm resistance heater by which the temperature was controlled. These components of the cryogenic system were directly connected to the inner portion of the cell that was surrounded by the outer can which thermally isolates the inner portion of the cell (see Figure 7). The inner portion is a cylinder with dimensions of 15 cm length and 5 cm diameter. The zinc sulfide infrared transparent windows, onto which the sample loading was done, sealed the two ends of the inner cell. The temperature measuring sensor was embedded in the cell wall near one window, so the temperature near the window will be cited throughout this discussion.

FT-IR Instrument

A Digilab FTS-20C model instrument was used to collect FT-IR absorbance spectra that were monitored, stored and manipulated on a Motorola PC. Since the FT-IR instrument was a single beam spectrometer, a background spectrum was obtained for each series of spectra.

Experimental Procedure

Preparation of a Network of Ice Nanocrystals

The window deposited nanocrystals method was used to create the networks of ice nanocrystals. Procedures for this method are as follows; H_2O (D_2O) vapor and carrier gas (N_2 (g)) were first loaded into the sample bulb so their molar ratio would be 1/100 (H_2O/N_2). After that, this gas mixture was loaded into the precooled cell (~68 K) with ~300 torr of the gaseous mixture from the one liter sample bulb expanded into the cell during each loading stage. A load-evacuation cycle was repeated ~60 times to complete formation of an assembly of the nanocrystals. The loading temperature of 68 K was held constant during the load-evacuation cycles. When the gas mixture goes into the cold inner cell, the water vapor in the 1% gas mixture becomes liquid droplets. On a short time scale, these liquid droplets crystallize and ~7% of the nanocrystals become attached to the windows of the cell. The thickness of the resulting network increases with the number of loadings, as observed with FT-IR spectroscopy as increasing peak intensities.

After the deposition was finished, the sample was annealed to 138 K. During the annealing process, small particles become larger by Ostwald ripening. The annealing temperature was chosen roughly 20 K higher than the planned reaction temperature so that the particle size remained stable during the reaction.

The most important characteristic for the ice nanocrystals was reproducibility. That is, when each network of the ice nanocrystals was prepared and then the FT-IR spectrum was collected, the same spectrum was obtained.

Adding NH_3 (ND_3) and Collecting FT-IR Spectra

After the ice nanocrystals were annealed, the temperature was decreased to the reaction temperature. Before adding NH_3 (ND_3), the bare ice spectrum was taken. Since the guideline for production of the monohydrate of ammonia was a one to one mole ratio of ammonia and ice, the same amount of ammonia as water in the nanocrystals was admitted. After NH_3 (ND_3) was added, the spectra of the ice nanocrystals were taken as a function of time. All spectra were collected by co-adding 400 scans at a nominal 4.0 cm^{-1} resolution.

Evaluation of the Data

To evaluate the rate data, the best ammonia monohydrate spectra were chosen as standard spectra for $NH_3.H_2O$, $NH_3.D_2O$ and $ND_3.D_2O$. The standard spectra were achieved from samples following complete reaction after several hours. In Figure 8, the standard spectra are shown for each monohydrate form. All data were evaluated according to these standard spectra as follows; two characteristic peak intensities for peaks marked ✳ were measured from the standard spectrum of each monohydrate and the ratio of these two peak intensities was found. Then, the bare ice spectrum was subtracted from spectra of partially reacted ice that were collected as a function of time until obtaining the same peak ratios. In Figure 9, one example of data evaluation is shown to help visualize the procedure. In that figure, the top spectrum is the bare H_2O ice spectrum and the middle one is the partially reacted ice spectrum that was taken after 3 hours of exposure to ammonia. From the standard spectrum of $NH_3.H_2O$, the ratio of 2900 and 3200 cm^{-1} peak intensities was known. When the bare H_2O ice spectrum is subtracted

22

from the partially reacted spectrum, the subtracted spectrum, which is the bottom one, was obtained as the monohydrate spectrum whose 2900 and 3200 cm^{-1} peak intensity ratio is equal to that ratio for the standard spectrum of $NH_3.H_2O$.

For kinetic analysis, the subtraction factors were the basic data. Since the subtraction factor equals the fraction of the unreacted ice, one minus the subtraction factor gives the reacted ice portion for a specific reaction time. Using these values, the reacted ice fractions could be plotted as a function of the reaction time.
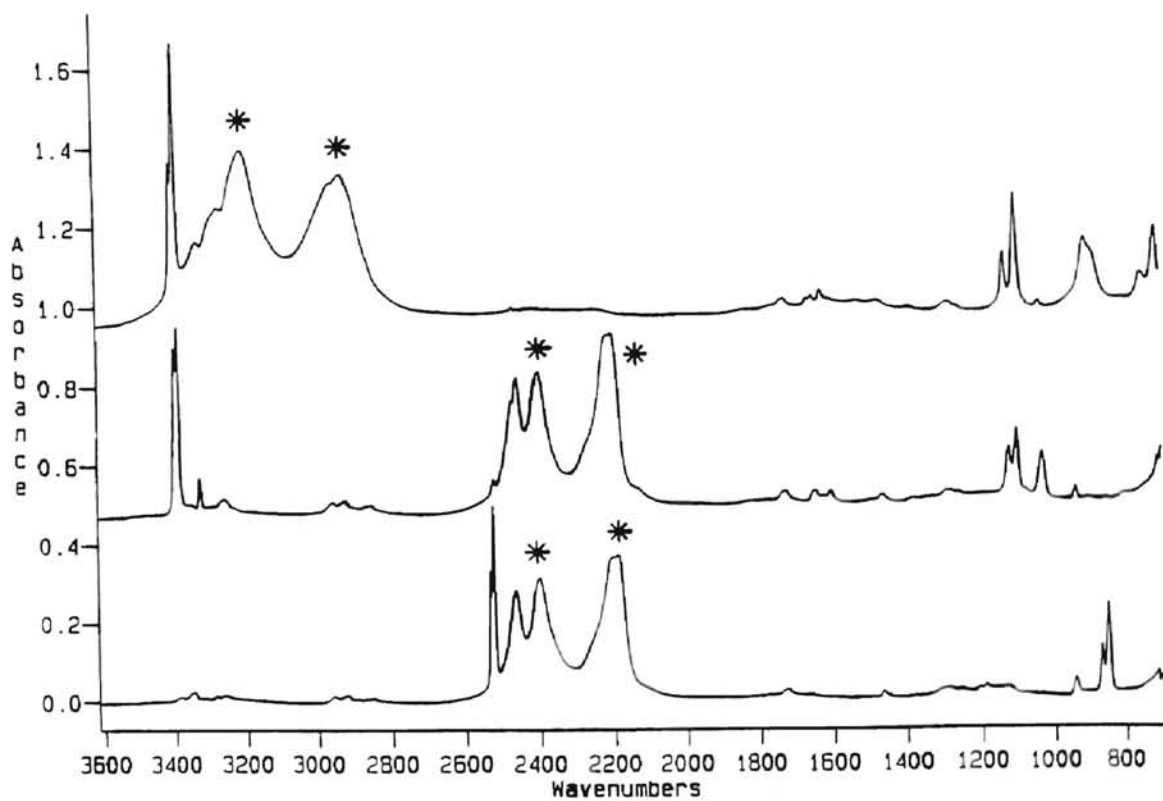
Figure 8. Standard spectra of $NH_3.H_2O$, $NH_3.D_2O$ and $ND_3.D_2O$ from top to bottom, respectively
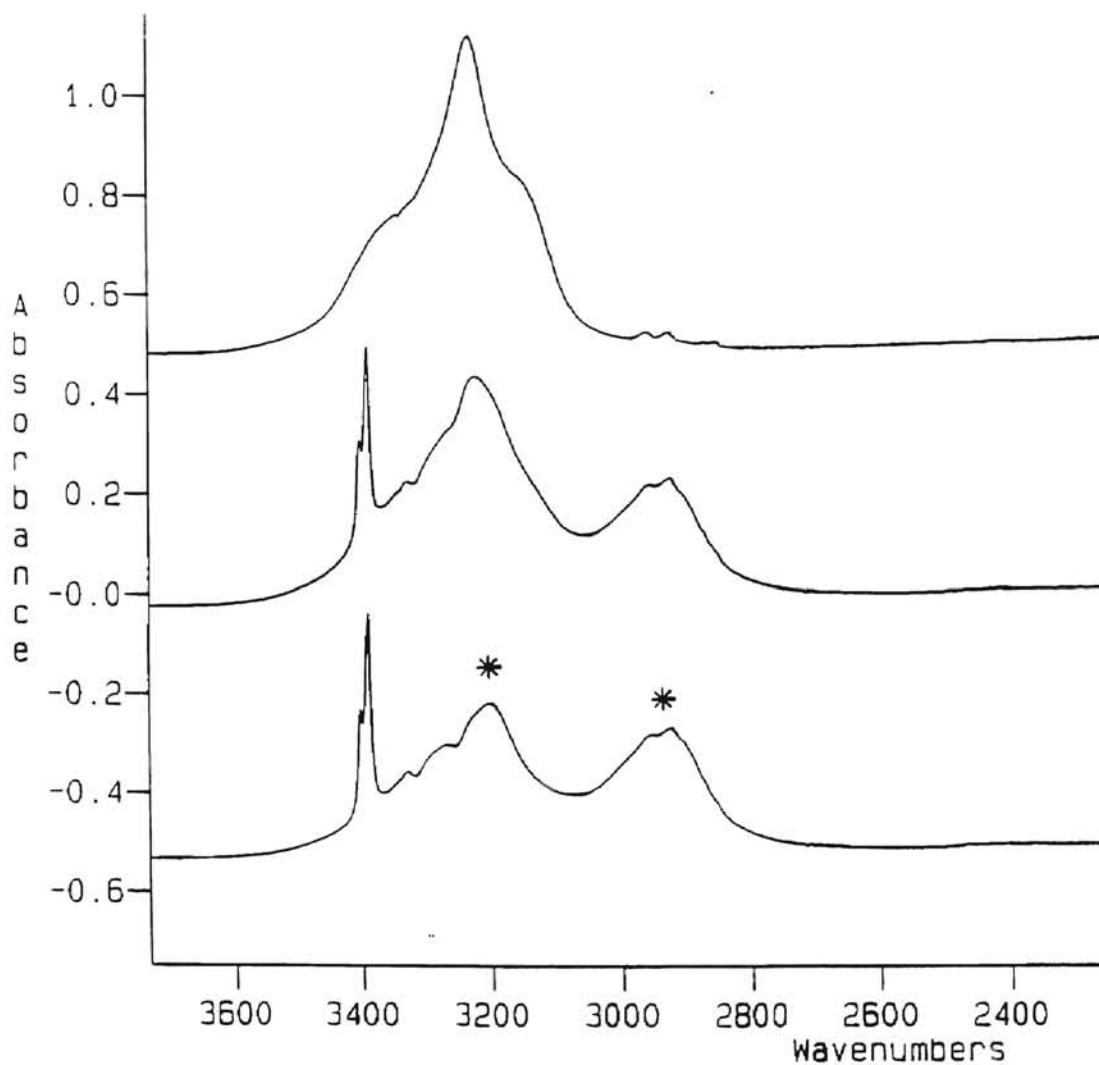
Figure 9. Finding one datum for extent of formation of $NH_3.H_2O$: top; the bare H_2O ice spectrum. middle; the partially NH_3 reacted ice spectrum (monohydrate spectrum + unreacted ice spectrum) and bottom: the subtracted spectrum (partially coated ice spectrum – bare ice spectrum) with * peak ratios of standard value for $NH_3.H_2O$

CHAPTER III

EXPERIMENTAL RESULTS AND DISCUSSION

Conversion of the Ice Nanocrystals to the Monohydrate of Ammonia and Mechanism for this Conversion

The ice nanocrystals were completely converted to the monohydrate of ammonia at cryogenic temperatures. The products of the conversions of H_2O and D_2O ice nanocrystals to a hydrate of ammonia were $NH_3.H_2O$, $NH_3.D_2O$ and $ND_3.D_2O$ and their FT-IR spectra are represented in Figure 10.

Evidence about the production of the monohydrate of ammonia can be found by comparing the spectra of $NH_3.H_2O$ and $ND_3.D_2O$ formed from ice nanocrystals and the published spectra of the bulk hydrate (see Figure 4 and Figure 5). The FT-IR spectrum of $NH_3.D_2O$ is not available in the literature. Although, we used an entirely different technique and much lower temperature, the comparison of the spectra shows that we obtained very similar spectra. Moreover, despite the statement of Bertie and Shehata[15] that the production of $NH_3.D_2O$ was impossible at low temperature, we managed to produce $NH_3.D_2O$ from the ice nanocrystals.

The conversion of the ice nanocrystals to the monohydrate of ammonia is a heterogeneous gas-solid process. However, when the ammonia is expanded into the cold cell (~120 K), it first condenses near the entry port of the cell. Since the reaction actually depended (indirectly) on the vapor pressure of NH_3 (ND_3), the cell temperature needed to be appropriate for a significant equilibrium vapor pressure of NH_3 or ND_3. Furthermore, the reaction temperature should be chosen as suitable for the reaction to be followed by
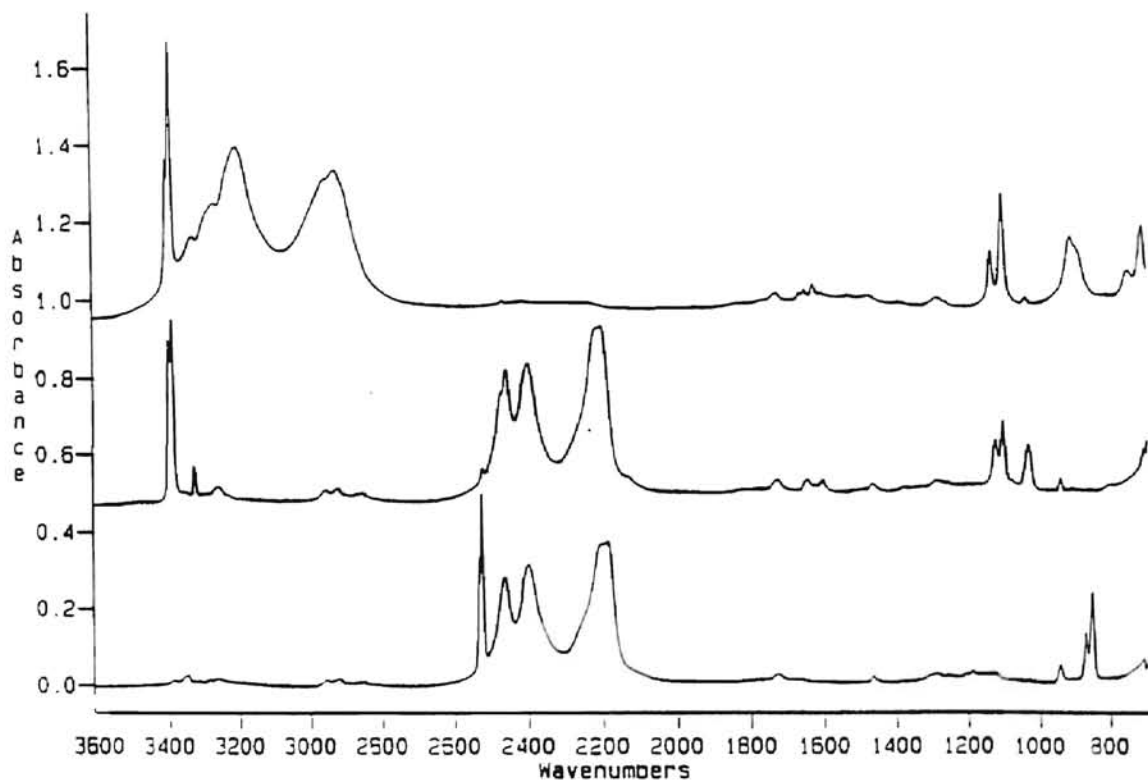
26

Figure 10. Spectra of $NH_3 \cdot H_2O$, $NH_3 \cdot D_2O$ and $ND_3 \cdot D_2O$ from top to bottom, respectively

FT-IR spectroscopy. At the beginning of this study, the NH_3-D_2O system was first studied and the temperature was chosen as 115 and then 117 K; but no reaction was observed.

Consequently, the reaction temperature was established as 120 K for NH_3-D_2O. The same temperature was used for NH_3-H_2O. Because of the vapor pressure isotope effect[25], the reaction temperature for the ND_3-D_2O system was raised to 123 K.

The conversion of the ice nanocrystals to the monohydrate of ammonia proceeds via a molecular mechanism as follows

$$NH_3(g) + H_2O(s) \longrightarrow NH_3.H_2O(s)$$

$$NH_3(g) + D_2O(s) \longrightarrow NH_3.D_2O(s)$$

$$ND_3(g) + D_2O(s) \longrightarrow ND_3.D_2O(s)$$

The indication for the molecular mechanism was that we did not observe any O-H band in the $NH_3.D_2O$ spectrum (see top and middle spectrum in Figure 10). If this reaction had proceeded via an ionic mechanism based upon formation of NH_3D^+ and OD^-, we would have observed isotopic hydrogen exchange between the NH_3 and D_2O molecules of the reacting ice, with HOD produced. OH bond modes in $ND_3.D_2O$[12] were defined in Table 1.

In the case of NH_3 and D_2O, we did observe the bands of NH_2D (1030 cm^{-1}) and ND_2H (940 cm^{-1})[12]. Figure 11 shows increasing deuteration of NH_3 with time of the reaction with D_2O in the bending region of $NH_3.D_2O$. It must be emphasized that these species apparently formed near the warmer entry port of the cell. After NH_2D and ND_2H formed in the condensed phase at the entry port of the cell, their vapor becomes available for reaction with the D_2O ice nanocrystals deposited on the windows. Therefore, we had
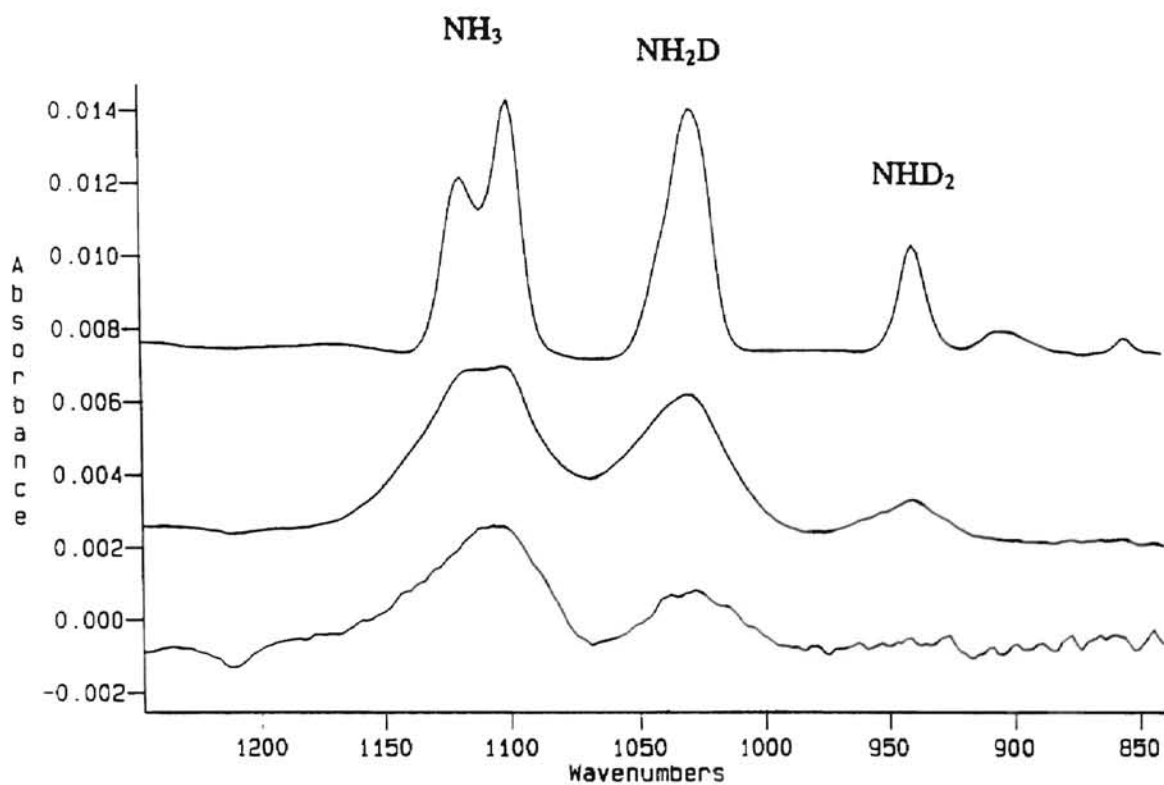
Figure 11. Spectra that show increase in deuterated isotopomers with time of reaction of NH_3 with D_2O in the bending region of $NH_3.D_2O$

also these reactions in the NH_3-D_2O system;

$$NH_2D(g) + D_2O(s) \longrightarrow NH_2D.D_2O(s)$$

$$ND_2H(g) + D_2O(s) \longrightarrow ND_2H.D_2O(s)$$

Although we observed the bands of these species, there was no isotopic exchange in D_2O part of monohydrate. That is, there are no OH bands in the spectrum of $NH_3.D_2O$ (see top and middle spectra in Figure 10).

Rate of Conversion of Ice Nanocrystals to the Monohydrate of Ammonia and Deuterium Isotope Effects on the Reaction Kinetics

The scaled difference spectrum between the spectra of partially NH_3 (ND_3) reacted ice and the spectra of the bare ice was used to obtain the rate for these reactions. Figures 12, 13 and 14 show the formation of $NH_3.D_2O$, $NH_3.H_2O$ and $ND_3.D_2O$ as a function of time, respectively. In these figures, each spectrum that corresponds to a specific reaction time has a subtraction factor equal to the fraction of the unreacted ice. Since the total fraction of ice is one, one minus the subtraction factor gives the fraction of the reacted ice.

The NH_3-H_2O and NH_3-D_2O systems will be examined firstly for the understanding of the deuterium isotope effect. For the consistency of the results, each experiment for the conversion to the monohydrate was repeated twice and then average values of the fractions of the reacted ice was calculated. Tables 1 and 2 show the fraction of the reacted ice with corresponding reaction time for $NH_3.H_2O$ and $NH_3.D_2O$, respectively.
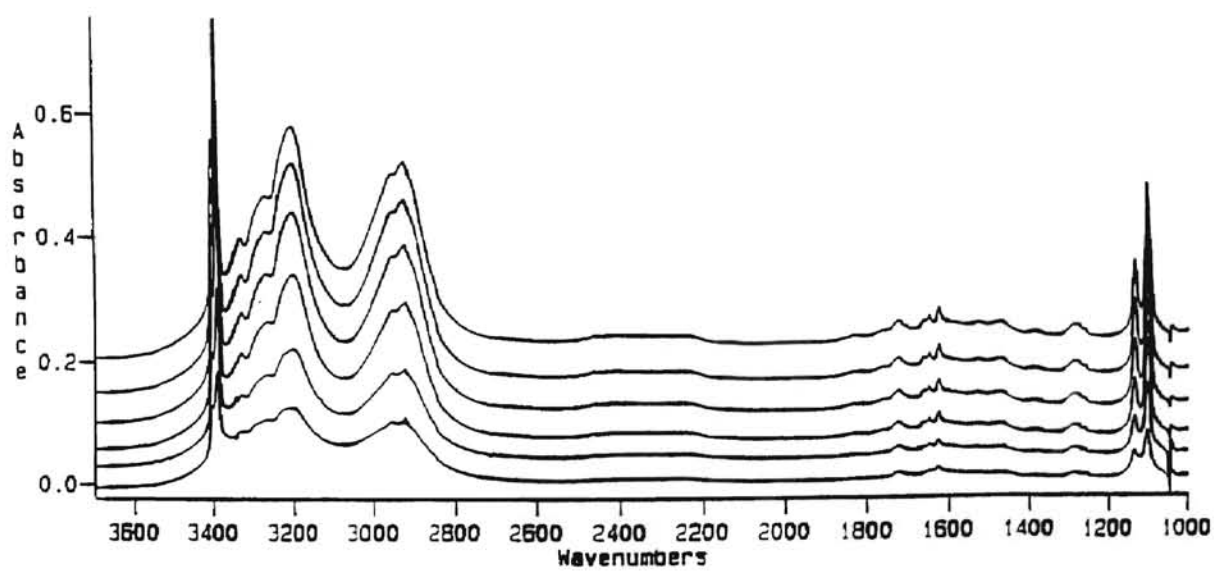
Figure 12. Conversion of H_2O ice to $NH_3.H_2O$ at 120 K as a function of time, from bottom to top, spectra of 2, 3, 4, 5, 6, 7 and 8 hours later reaction, respectively
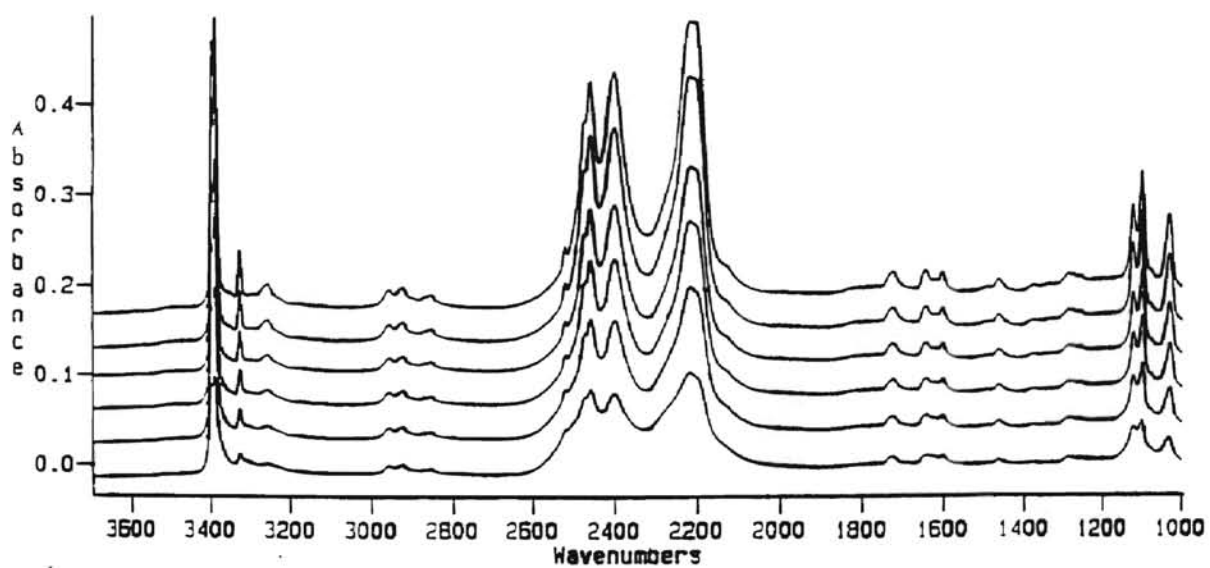
Figure 13. Conversion of D_2O ice to $NH_3.D_2O$ at 120 K as a function of time, from bottom to top, spectra of 3, 4, 5, 6, 7 and 8 hours later reaction, respectively
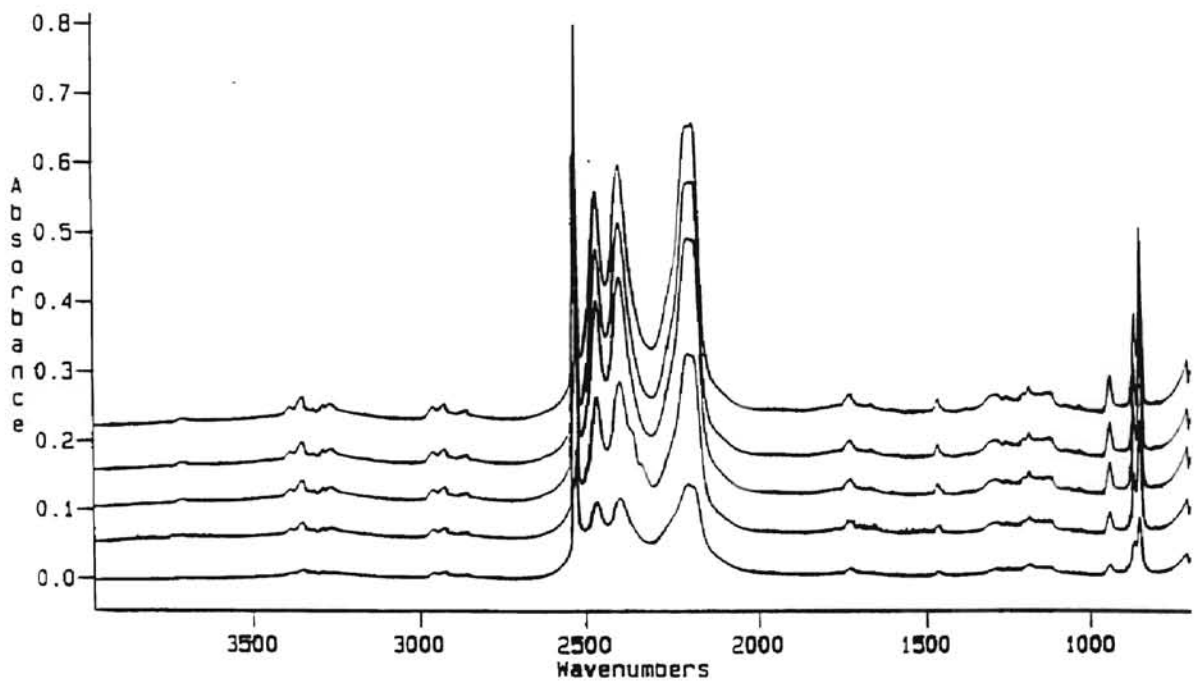
Figure 14. Conversion of D_2O ice to the $ND_3.D_2O$ at 123 K as a function of time, from bottom to top, spectra of 3, 4, 5, 6 and 7 hours later reaction, respectively

Table 2

Experimental Results for $NH_3.H_2O$ at 120 K

Time (hr)	Fraction of reacted ice for $NH_3.H_2O$
2	0.38
3	0.55 ·
4	0.73
5	0.88
6	0.94
7	0.96

Table 3

Experimental Results for $NH_3.D_2O$ at 120 K

Time (hr)	Fraction of reacted ice for $NH_3.D_2O$
3	0.35
4	0.47
5	0.60
6	0.71
6.2	0.79
7	0.86
8	0.96

A plot of these values with corresponding reaction time is given by Figure 15 (in the case of $NH_3.D_2O$, because of the time difference, the fractions of the reacted ice in 6 and 6.2 hours could not be averaged, but they are shown separately in the Figure 15). In Figure 15, after starting point (zero time vs. zero reacted ice), we did not have any value until 2 hours for $NH_3.H_2O$ and 3 hours for $NH_3.D_2O$. The reason for this was that at the beginning of the reaction, the amorphous structures of the monohydrate product were dominant so that resolution of the spectra into ice and hydrate components using the standard monohydrate spectra was not possible.

Although the linear plot was obtained for $NH_3.D_2O$, the plot was curved for $NH_3.H_2O$ after 5 hours. This may indicate "saturation kinetics". When the fraction of the reacted ice in the graph of $NH_3.H_2O$ approached one, the line became curved because the final fraction of the reacted ice is one. Since the rate for the NH_3-D_2O system was slow, we did not observe saturation effect for the NH_3-D_2O system in this time range. However, if the plotting was kept going for the NH_3-D_2O system, it would be curved due to the saturation effect.

The reaction rate, in general, depends on the diffusion of ammonia molecules to the ice particles through the crust of hydrate that has formed. Because ammonia molecules must also penetrate the ice to form hydrate, this is not a simple diffusion. Although knowledge of the available amount of NH_3 (g) for the diffusion was essential for analyzing these conversions, because of the equilibrium (shown below) between the solid and gas phase of ammonia, this amount could be considered as a constant during the reactions. (The vapor pressure of ammonia at 120 K was measured as 10^{-3} Torr.)

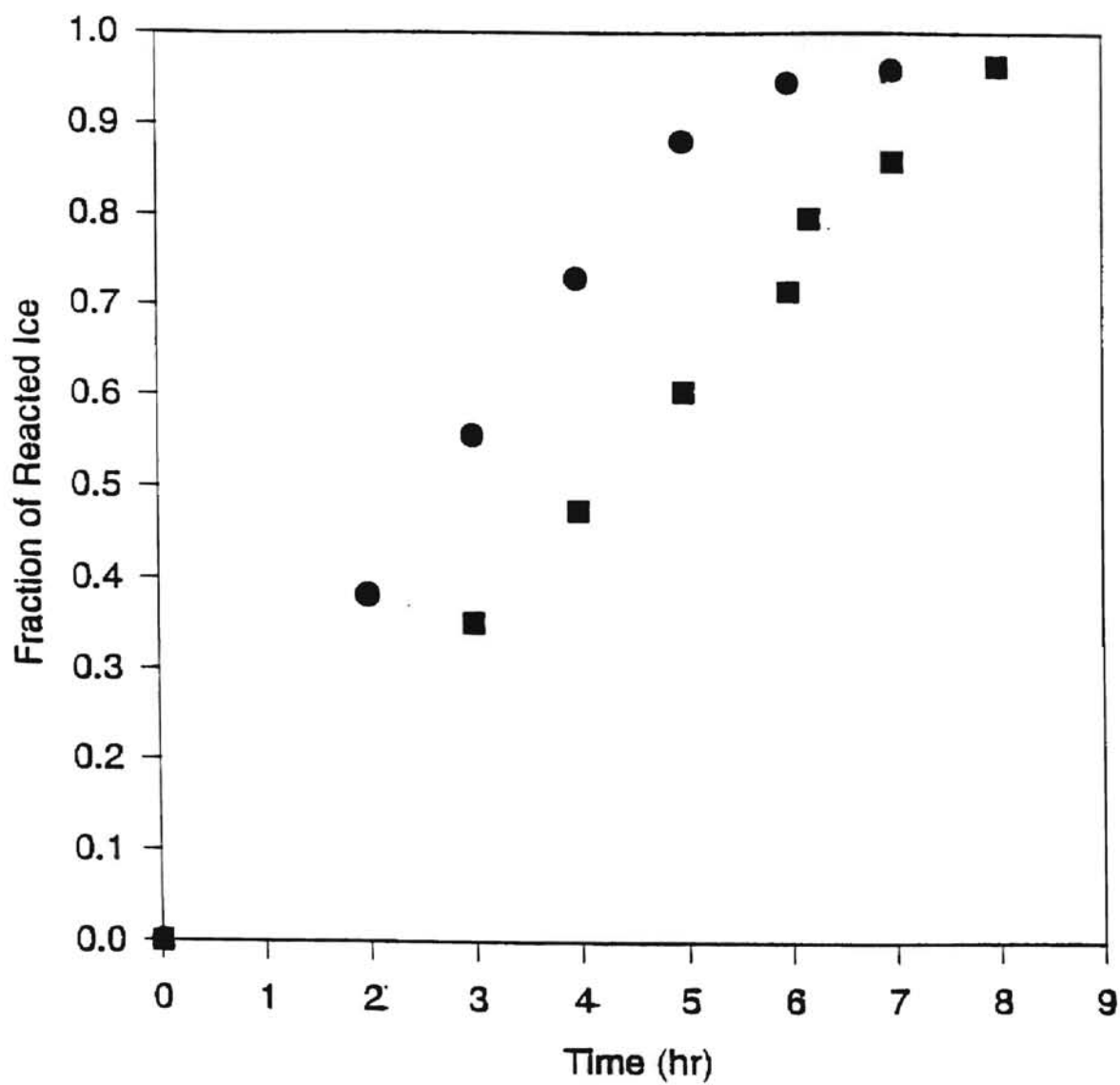$$NH_3 \text{ (s)} \rightleftharpoons NH_3 \text{ (g)}$$

Figure 15. Comparison of the formation rates for two monohydrates of ammonia
● for conversion of H_2O ice nanocrystals to $NH_3.H_2O$ at 120 K
■ for conversion of D_2O ice nanocrystals to $NH_3.D_2O$ at 120 K

In Figure 15, the reaction for $NH_3.H_2O$ followed a linear plot for several hours of reaction and the plot was linear for $NH_3.D_2O$. From this standpoint, one could say the reaction for both forms of monohydrate proceeded with pseudo zero order kinetics.

Analysis Assuming P_{NH3} is Rate Limiting Factor

When NH_3 is expanded into the cold cell, it condenses at the cold entry port of the cell, which is warmer than other parts of the cell. Then, it starts to vaporize and moves to the wall of inner cell (the coldest part of the cell) containing also ice particles (see Figure 16 A). First a tightly adsorbate monolayer forms on the ice. After that, as a polylayer of NH_3 forms, the vapor pressure becomes significant so the NH_3 begins to move through the network of ice nanocrystals deposited on the window (see figure 16 B).

Since a basic parameter for these reactions is the vapor pressure of ammonia that is a constant, the concentration of ammonia molecules in the gas phase may control the rate of this zero order reaction. With simple assumptions, a mechanism of the rate of the reaction can be suggested as follows: it may be assumed an imaginary boundary exists between the gas phase of ammonia and the network of the ice nanocrystals as in Figure 16 B. Any NH_3 molecule crossing this boundary must collide with a nanocrystal and, assuming an accommodation coefficient of 1.0, become attached to a particle. From this point of view, the rate of the reaction is apparently equal to the number of the ammonia molecules crossing this imaginary boundary.

Since the number of ammonia molecules crossing this boundary depends on the vapor pressure of ammonia and the wall temperature (120 K), the vapor pressure of ammonia can be calculated by rate of NH_3 coating of the ice surface. The crossing of this
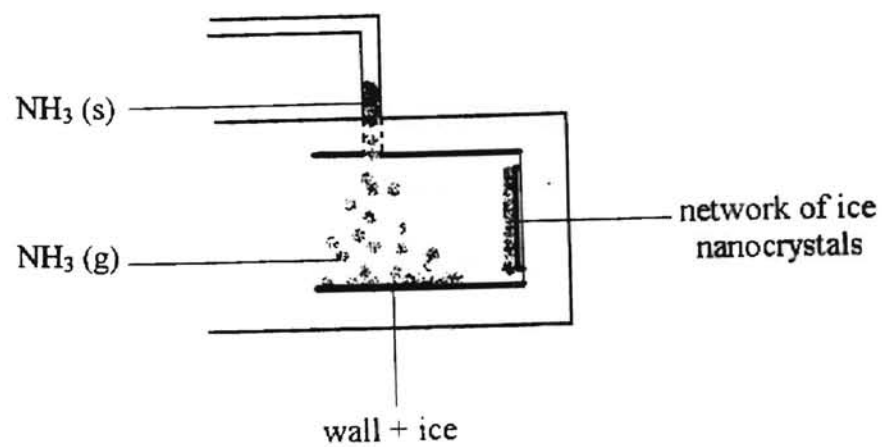
A
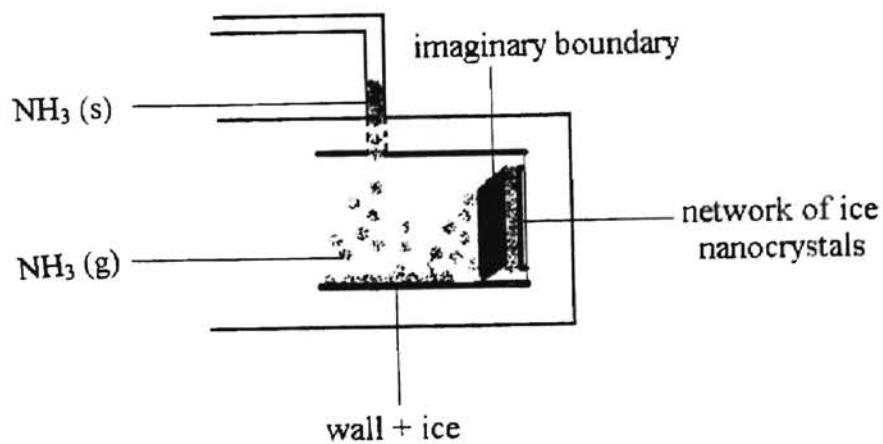
B

Figure 16. A simple picture of the mechanism of the transport of NH$_3$ to the ice nanocrystals.

boundary by NH_3 molecules can be examined in terms of the number of collisions per

unit area per unit time that is given by the following equation;[27]

$$Z = \frac{P}{(2\pi m k T)^{1/2}}$$

where Z is the number of collisions per unit area per unit time, P is the pressure in unit of

pascal (Pa), m is molecular mass of one particle (m = M / N, where M is the molar mass

of the molecule, N is the Avogadro's constant), k is the Boltzman constant, T is the

temperature. By using this equation, we can calculate a pressure of ammonia from the

experimental result. For this calculation, the experimental results of the NH_3-H_2O system

will be used.

From the above assumptions, it can be written:

the number of collisions with boundary = the number of product molecules

= the number of the reacted H_2O ice molecules.

From the experimental result, to find the number of reacted ice molecules, we should

calculate the total initial amount of the ice by using the following equation and the

observed absorbance spectrum;[28]

$$A = \varepsilon (v) \, l \, / \, 2.303 = \log (I_0 (v) / I (v))$$

where A is the absorbance, ε is the absorptivity at the frequency of v, l is the thickness of

the sample, $I_0 (v)$ and $I (v)$ are the intensities of the light before and after traversing the

distance l, respectively. The average absorbance for the two experiments of the H_2O ice

at 3220 cm^{-1} was measured as 0.642. Bertie et al.[28] studied the absorptivity of ice I in range 4000-30 cm^{-1} and they calculated the absorptivity of H_2O ice at 3220 cm^{-1} as 33.0×10^3 cm^{-1}. Substituting these values into the absorbance equation gives the thickness of the ice as 4.48×10^{-5} cm.

The slope for the linear part of the plot in Figure 15 for $NH_3.H_2O$ is found as ~0.17 and is equal to k, the rate constant, in units of the fraction of the reacted ice per unit time (hr). From here, we can find the fraction of the reacted ice per second as $~4.7 \times 10^{-5}$.

Since the density of ice[29] is 0.92 gr/cm^3, multiplying the density by the thickness gives the amount of the ice per square centimeter as $~4.12 \times 10^{-5}$ gr/cm^2.

Multiplying the fraction of the ice per second (4.7×10^{-5} per sec.) by the amount of the ice per square centimeter (4.12×10^{-5} gr/cm^2) gives $~1.93 \times 10^{-9}$ in units of gr/sec.cm^2. By using Avogadro's constant, we obtain $~6.4 \times 10^{13}$ as the number of reacted ice molecules per second per square centimeter which is assumed equal to the number of boundary collisions (Z). Putting these values into the Z equation gives the pressure of ammonia as $~1.09 \times 10^{-5}$ Pa (Nm^{-2}) or 8.17×10^{-8} Torr.

Although we measured the vapor pressure of NH_3 as 1×10^{-3} Torr, this was an approximate measurement. However, we can calculate the vapor pressure of NH_3 at 120 K by using the equation given by[30].

$$\log P_{NH_3} = - (1630.700 / T) + 9.00593$$

where P_{NH_3} is the vapor pressure of NH_3 (s) (cm of Hg) at the temperature T. By substituting 120 K into this equation, the pressure of ammonia at 120 K is found as 2.61×10^{-4} torr.

When we compare 1×10^{-3} torr (from measurement), 2.61×10^{-4} torr (from calculation) and 8.17×10^{-8} torr (from experimental result), we can see the difference between the vapor pressure from measurement or calculation and from the experimental result assuming unit reaction probability for molecules that cross the boundary. It follows that the NH_3 (g) vapor pressure cannot be the rate controlling factor.

Crossing the NH_3 (s)-Ice Barrier as the Rate Limiting Step

We may explain this difference as follows: since the entry port of the cell where the NH_3 originally condenses is warmer than the inside (including the cell windows), after crossing the imaginary boundary, the ammonia molecules condense much more rapidly than they can react with the network of ice. Thus, the reaction becomes a solid-solid reaction between NH_3 and the nanocrystals. From this view, we can explain why we calculate the vapor pressure of ammonia from the reaction rate to be orders of magnitude lower than from the calculation or measurement. Also, from this view the zero order reaction kinetics reflects the constant activity of NH_3 (s), and the reaction rate is controlled by the barrier for transport of NH_3 out of the NH_3 (s).

However, if the reaction rate is limited by transport from the solid ammonia, there should be no deuterium isotope effect for NH_3 reacting with H_2O versus D_2O. The slope for the linear part of the plot for $NH_3.H_2O$ was found above as ~0.17 and the slope for the plot for $NH_3.D_2O$ was calculated as ~0.12. If there is no deuterium isotope effect or zero point energy effect on the reaction kinetics, the two reactions should have proceeded with the same rate. However, as seen from Figure 15, or comparison of the slopes, NH_3 reacted with H_2O ice faster than with D_2O ice.

The difference may have occurred in their rates because, in the case of $NH_3.D_2O$. in addition to NH_3, there were also NH_2D and ND_2H species present (formation of these species was explained above) to participate in the conversion of D_2O to the monohydrate. The presence of these species would decrease the total chemical activity of the solid ammonia. Consequently, existence of these species may have reduced the rate for the conversion of D_2O ice to $NH_xD_{3-x}.D_2O$.

When only NH_3 was replaced by ND_3, without changing the D_2O ice, and each fraction of the reacted ice amount was found (shown Table 4), like above, and plotted as a function of time for the conversion of D_2O ice to $ND_3.D_2O$, the plot shown in Figure 17 was obtained.

Table 4

Experimental Results for $ND_3.D_2O$ at 123 K

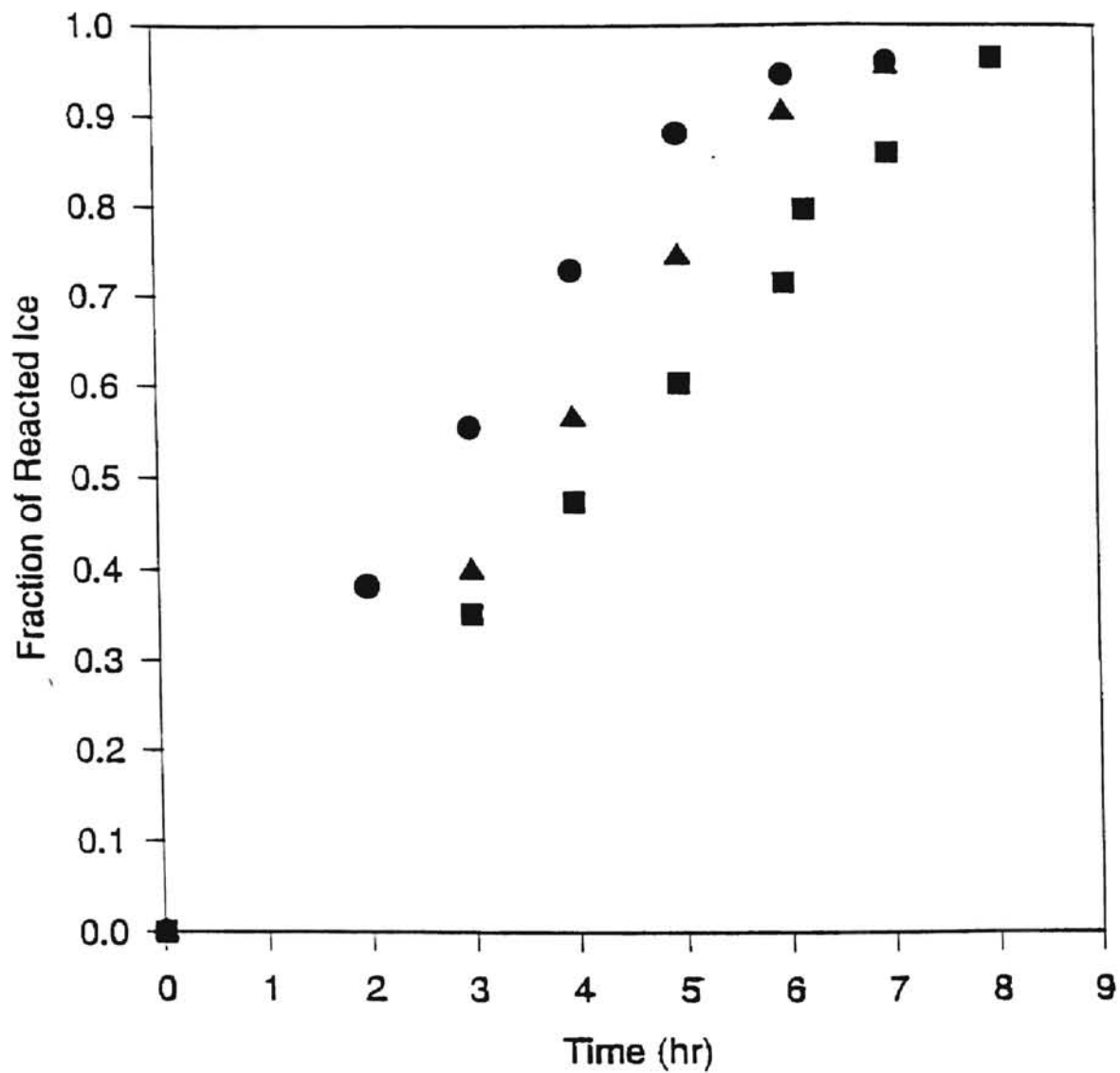| Time (hr)	Fraction of reacted ice for $ND_3.D_2O$
3	0.39
4	0.56
5	0.74
6	0.90
7	0.95

Figure 17. Comparison of the formation rates for three monohydrates of ammonia
● for conversion of H_2O ice nanocrystals to $NH_3.H_2O$ at 120 K
▲ for conversion of D_2O ice nanocrystals to $ND_3.D_2O$ at 123 K
■ for conversion of D_2O ice nanocrystals to $NH_3.D_2O$ at 120 K

In the case of $ND_3.D_2O$, only one set of rate measurement values was used because of temperature problems with the other set. Although a higher temperature was used for $ND_3.D_2O$, its rate plot is shown superimposed on the same plot for $NH_3.H_2O$ and $NH_3.D_2O$. We observed again the saturation point for $ND_3.D_2O$ after the 6th hour of reaction. Moreover, in the case of $ND_3.D_2O$, the reaction again proceeded with pseudo-zero order kinetics for several hours reaction time. In addition, the slope for the linear part of the plot was found as ~0.17.

The same mechanism is expected to be valid for the formation of $ND_3.D_2O$ as for the other monohydrates. However, since ND_3 (s) is more stable than NH_3 (s) (because of the fact that a molecule with deuterium has lower zero point lattice vibrational energy than with hydrogen), the activation energy for the reaction with ND_3 is higher than that for the reaction with NH_3. In other words, at the same temperature, the chemical activity of ND_3 (s) is lower than of NH_3 (s). For example, the relation between the vapor pressures is given by the following equation;[25]

$$\log (P_{NH3} / P_{ND3}) = (49.69 / T) - 0.1305$$

For the vapor pressure of ND_3, the following equation can be used;[25]

$$\log P_{ND3} \text{ (cm of Hg)} = -(1680.4 / T) + 9.1364$$

And from this equation, it is found that P_{ND3} is equal to 1.35×10^{-4} torr at 120 K (P_{NH3} was calculated at page 40 as 2.61×10^{-4} torr at the same temperature). Therefore, we increased the temperature by 3 K to obtain the same vapor pressure for the ND_3-D_2O system as the NH_3-H_2O (D_2O) system.

44

The zero order kinetics indicates the constant chemical activity of solid ammonia at a given temperature where the chemical activity is equal to the multiplication of concentration and chemical activity coefficient which is a function of temperature. As seen, comparison of the slopes for $NH_3.H_2O$ (k = ~0.17) and $ND_3.D_2O$ (k = ~0.17), we obtained the same rate constant after this 3 K increase in T for the latter case. This may indicate that this 3 K increase may make the chemical activity of ND_3 (s) nearly equal to the chemical activity of NH_3 (s). Therefore, the reaction rates for NH_3 and ND_3 reacting with H_2O and D_2O at 120 and 123 K, respectively, become nearly equal to each other.

Moreover, this result is also evidence that there is no deuterium isotope effect for H_2O versus D_2O when the systems of NH_3-H_2O and ND_3-D_2O are compared.

Major Sources of Errors in Determination of the Reaction Rates

We now try to answer this question: what are the sources of errors for rate values represented in Figure 17?

Although, we minimized the temperature stability problem by doing these experiments without stopping, from beginning of the reaction to end of the reaction, it was impossible to hold the temperature precisely at 120 K (or 123 K) throughout the several hours of reaction. Although, each spectrum was taken at the chosen reaction temperature, sometimes a temporary variation of ~one K was noted during the reaction. If the reaction is activated, a temperature increase or decrease affects the rate of the reaction. Since this variation is temporary, we cannot estimate the magnitude of its effect. However, the possibility of a one K variation in temperature can be considered as an error source to make questionable the observed isotope effect.

A second source of error is the pressure of residual noncondensible gasses (the components of air, such as nitrogen, oxygen, carbon dioxide, argon and so on) in the reaction system. The difference between the vapor pressures obtained from the measurement (1×10^{-3} torr) and calculation (2.64×10^{-4} torr) may indicate the existence of residual gasses. Since the presence of the residual gasses reduces the vapor transport of ammonia, the reaction rate could be influenced. We cannot say anything about the magnitude of this error. However, it must be noted here as a potential error source.

A third source of error is in the spectroscopic measurements. To find the rate values represented in Figure 17, we used the intensities of the peaks (as explained in the evaluation of data section). Although we made the base line corrections to measure accurately these peak intensities, since these were broad peaks (as seen in Figure 8, 12, 13 and 14), some errors might come from the measurement of these peak intensities.

Future Research

Since the rate determining step for the reaction of ammonia with ice nanocrystals apparently involved the transport of ammonia from the solid ammonia or a larger of adsorbed NH_3, the isotope effect for NH_3 and ND_3 can be found as k_{NH3}/k_{ND3} by using the same reaction temperature and analyzed in terms of isotope ratio theories. Also a range of temperatures may be used to determine activation energy of the reaction. Further, the activation energies can be found from the theoretical simulation of the molecular-level mechanism and compared to the experimental values.

Moreover, we tried to find rate and isotope effects for conversion of ice nanocrystals to the monohydrate of ammonia in this study and we observed a molecular

mechanism for this conversion. As mentioned in the literature review, ethylene oxide (EO) also converts the ice nanocrystals to the type I clathrate hydrate via a molecular mechanism at the cryogenic temperatures. A similar study can be made of the rate and isotope effects for this conversion.

Summary

Interaction of NH_3 (ND_3), a penetrating adsorbate of H_2O (D_2O) ice nanocrystals as monitored by FT-IR spectroscopy, results in the formation of $NH_3.H_2O$, $NH_3.D_2O$ and $ND_3.D_2O$. It was found that the conversion of the ice nanocrystals to these monohydrates proceeded via a molecular mechanism.

Since these conversions occur through a heterogeneous gas solid process, the rate for these conversions could depend directly on the vapor pressure of ammonia at the reaction temperature. Because there was an equilibrium between the solid and gas phase of ammonia, the amount of ammonia in the gas phase was considered a constant during the reaction. It was found that the conversion of the ice nanocrystals to the monohydrate of ammonia proceeded with zero order kinetics, but was much to slow to be limited by the transport of ammonia across an imaginary boundary between the gas phase of ammonia and the network of the ice nanocrystals.

Rather a more reasonable view is that the rate limiting stage involves the transport of ammonia from NH_3 (s) into the ice/hydrate. If such transport is dependent on the barrier for NH_3 leaving the solid ammonia, it could cause an activated zero order reaction with no water isotope effect, as observed.

REFERENCES

1. Lunine, J. I., "Chemistry in the Outer Solar System." C&EN, Special Report, p. 41, 1995.

2. Lewis, J. S., "The Clouds of Jupiter and the NH_3-H_2O and NH_3-H_2S Systems." Icarus, Vol. 10, p. 365, 1969.

3. Lewis, J. S., "Satellites of the Outer Planets: Their Physical and Chemical Nature." Icarus, Vol. 15, p. 174, 1971.

4. Rowland, B., Kadagathur. N. S., Devlin, J. P., Buch, V., Feldeman, T., and Wojcik, M. J., "Infrared Spectra of Ice Surfaces and Assignment of Surface-Localized Modes from Simulated Spectra of Cubic Ice." J. Chem. Phys., Vol. 102, p. 8328, 1995.

5. Devlin, J. P. and Buch, V., "Surface of Ice as Viewed from Combined Spectroscopic and Computer Modeling Studies." J. Phys. Chem., Vol. 99, p. 16534, 1995.

6. Rowland, B., Kadagathur. N. S., and Devlin, J. P., "Infrared Spectra of CH_4 Adsorbed on Ice: Probing Adsorbate Dilution and Phase Separation with the v_3 Transverse-Longitudinal Splitting." J. Chem. Phys., Vol. 102, p. 13, 1995.

7. Rowland, B., Devlin, J. P., and Buch, V., $(H_2O)_{20}$, Simulated $(H_2O)_{450}$ and Ice Nanocrystal Spectra Compared. (unpublished)

8. Delzeit, L., Devlin, M. S., Rowland, B., Devlin, J. P., and Buch, V., "Adsorbate-Induced Partial Ordering of the Irregular Surface and Subsurface of Crystalline Ice." J. Phys. Chem., Vol. 100, p. 10076, 1996.

9. Rowland, B., Fisher, M. and Devlin, J. P., "Probing Icy Surfaces with the Dangling-OH-Mode Absorption: Large Ice Clusters and Microporous Amorphous Ice." J. Chem. Phys., Vol. 95, p.1378, 1991.

10. Delzeit, L., Powell, K., Uras, N., and Devlin, J.P., "Ice Surface Reactions with Acids and Bases." J. Phys. Chem. B, Vol. 101, p. 2327, 1997.

11. Devlin, J. P. and Buch, V., "FT-IR Spectra of Nano Particles: Surface and Adsorbate Modes." Mikrochimica Acta, Vol. 14, p. 57, 1997.

12. Devlin, J. P. and Buch, V., "Vibrational Spectroscopy and Modeling of the Ice Surface and of Ice-Adsorbate Interactions." J. Phys. Chem., in press, 1997.

13. Delzeit, L., Thesis, Oklahoma State University, 1997.

14. Langlet, J., Caillet, J. and Caffarel, M., "A Perturbational Study of Some Hydrogen-Bonded Dimers." J. Chem. Phys. Vol. 103, p. 8043, 1995.

15. Bertie, J. E. and Shehata, M. R., "The Infrared Spectra of $NH_3.H_2O$ and $ND_3.D_2O$ at 100 K." J. Chem. Phys. Vol. 83, p. 1449, 1985.

16. Bertie, J. E. and Devlin, J. P., "The infrared spectra and phase transitions of pure and isotopically impure $2ND_3.H_2O$, $2NH_3.D_2O$, $2NH_3.H_2O$ and $2ND_3.D_2O$ between 100 and 15 K." J. Chem. Phys., Vol. 81, p. 1559, 1984.

17. Szafran, M. and Dega-Szafran, Z., "A Critical Review of the Isotope Effect in IR Spectra." Journal of Molecular Structure, Vol. 321, p. 57, 1994.

18. Wolff, H., Rollar, H. G. and Wolff, E., "Infrared Spectra and Vapor Pressure Isotope effect of Crystallized Ammonia and Its Deuterium Derivatives." J. Chem. Phys., Vol. 55, p. 1373, 1971.

19. Melander, L., "Isotope Effects on Reaction Rates." New York: The Ronald Press Company; 1960.

20. Bigeleisen, J., "The Relative Reaction Velocities of Isotopic Molecules." J. Chem. Phys., Vol. 17, p. 675, 1949.

21. Bigeleisen, J. and Mayer, M. G., "Calculation of Equilibrium Constants for Isotopic Exchange Reactions." J. Chem. Phys., Vol. 15, p. 261, 1947.

22. Wiberg, K. B., "The Deuterium Isotope Effect." Chem. Revs. Vol. 55, p. 713, 1955.

23. Kaplan, L. and Wilzbach, K. E., " Hydrogen Isotope Effects in the Alkaline Cleavage of Triorganosilanes." J.Am. Chem. Soc., Vol. 77, p. 1297, 1955.

24. Westheimer, F. H., " The Magnitude of the Primary Kinetic Isotope Effect for Compounds of Hydrogen and Deuterium." Chem. Revs., Vol. 61, p. 265, 1961.

25. Kirshenbaum, I. and Urey, H. C., "The Difference in the Vapor Pressures, Heats of Vaporization, and Triple Points of Nitrogen (14) and Nitrogen (15) and Ammonia and Trideuteroammonia." J. Chem. Phys., Vol. 10, p. 706, 1942.

26. Shiner, V. J. Jr., "Deuterium Isotope Effects and Hyperconjugation." Tetrahedron, Vol. 5, p. 243, 1959.

27. Atkins, P. W., "Physical Chemistry." New York: W. H. Freeman and Company; 1994, p. 818.

28. Bertie, J. E., Labbe, H. J. and Whalley, E., "Absorptivity of Ice I in the Range 4000-30 cm^{-1}." J. Chem. Phys., Vol. 50, p. 4501, 1969.

29. Eisenberg, D. and Kauzmann, W., "The Structure and Properties of Water." London: Oxford University Press; 1969.

30. Overstreet, R and Giauque, W. F., "Ammonia. The Heat Capacity and Vapor Pressure of Solid and Liquid. Heat of Vaporization. The Entropy Values from Thermal and Spectroscopic Data." J. Am. Chem. Soc., Vol. 59, p. 254, 1937.

VITA

Nevin Uras

Candidate for the Degree of

Master of Science

Thesis: RATE AND ISOTOPIC EFFECTS FOR CONVERSION OF ICE
NANOCRYSTALS TO THE AMMONIA MONOHYDRATE

Major Field: Chemistry

Biographical:

Personal Data: Born in Pamukova, Sakarya, Turkey, On June 26, 1972, the daughter
of Ismail and Mukaddes Uras.

Education: Graduated from Pamukova High School, Pamukova, Sakarya, Turkey in
June 1989; received Bachelor of Science degree in Chemistry from Anadolu
University, Eskisehir, Turkey in October 1989 and June 1993, respectively.
Completed the requirements for the Master of Science degree with a major
in Chemistry at Oklahoma State University in July, 1997.